

# ATP conformations and ion binding modes in the active site of anthrax edema factor: A computational analysis

Leandro Martínez, Elodie Laine, Thérèse E. Malliavin,\* Michael Nilges, and Arnaud Blondel

Unité de Bioinformatique Structurale, URA CNRS 2185, Institut Pasteur, Paris, France

## ABSTRACT

The Edema Factor (EF), one of the virulence factors of anthrax, is an adenyl cyclase that promotes the overproduction of cyclic-AMP (cAMP) from ATP, and therefore perturbs cell signaling. Crystallographic structures of EF bound to ATP analogs and reaction products, cyclic-AMP, and Pyrophosphate (PPi), revealed different substrate conformations and catalytic-cation binding modes, one or two cations being observed in the active site. To shed light into the biological significance of these crystallographic structures, the energetics, geometry, and dynamics of the active site are analyzed using molecular dynamics simulations. The ATP conformation observed in the one-metal-ion structure allows stronger interactions with the catalytic ion, and ATP is more restrained than in the structure containing two Mg<sup>2+</sup> ions. Therefore, we propose that the conformation observed in the one-ion crystal structure is a more probable starting point for the reaction. The simulations also suggest that a C3'-endo sugar pucker facilitates nucleophilic attack. Additionally, the two-cation binding mode restrains the mobility of the reaction products, and thus their tendency to dissociate.

Proteins 2009; 77:971–983.  
© 2009 Wiley-Liss, Inc.

**Key words:** molecular dynamics simulation; anthrax; edema factor; cAMP; adenyl cyclase.

## INTRODUCTION

Anthrax releases three virulence factors when it infects host cells: Protective Antigen (PA), Lethal Factor (LF), and Edema Factor (EF). PA binds to the cell surface and to either LF or EF. The complexes are invaginated, and PA releases EF in the cytoplasm. EF then forms a calcium-dependent complex with Calmodulin (CaM) of the host, which activates it as an adenyl cyclase (AC). The structural rearrangement of EF upon CaM binding<sup>1</sup> shapes a mostly solvent-exposed catalytic site that binds ATP and converts it into cyclic-AMP (cAMP) and Pyrophosphate (PPi). As cAMP is an essential signaling molecule, its overproduction leads to uncontrolled fluid permeation and, consequently, edema formation in the infected organisms.

Tang and coworkers<sup>1–3</sup> have studied the molecular basis of EF activation and function and determined several crystallographic structures of EF in various conditions. Upon CaM binding, the helical domain of EF moves apart from the core of the structure, resulting in the intercalation of CaM within EF [Fig. 1(a)]. A large reorganization of switches A, B, and C, located at the interface between the helical and catalytic domains occurs simultaneously. This moves switches B and C in their conformation to form the active catalytic site.

The activity of the EF-CaM complex is dependent on the binding of ions at different sites in the structure. In particular, the binding of Ca<sup>2+</sup> to CaM is required for CaM and EF association. We have studied the effect of the level of Ca<sup>2+</sup> on the dynamics of EF-CaM previously.<sup>4</sup> CaM acts as a spring to maintain EF open: the stability of the inter-linker between the two CaM lobes is essential, and depends on Calcium binding on the C-terminal lobe. CaM best fits EF when two Ca<sup>2+</sup> are bound to its C-terminal lobes, and the two Ca<sup>2+</sup> binding sites of its N-terminal lobes are free.

In this work, we focus on another aspect of the structure and plasticity of the EF-CaM complex: the cation, substrate, and product configurations in the catalytic site and their role in enzyme activity. Indeed, the crystallographic structures solved to date exhibit several cationic binding modes and different substrate conformations,<sup>1–3,5</sup> providing multiple possible interpretations of EF's catalytic mechanism and its relation with those of Mammalian Adenyl Cyclases (MACs).<sup>6</sup>

The X-ray crystallographic structures of the EF-CaM complex give information about two different states of the catalytic site: (i) the state before the enzymatic

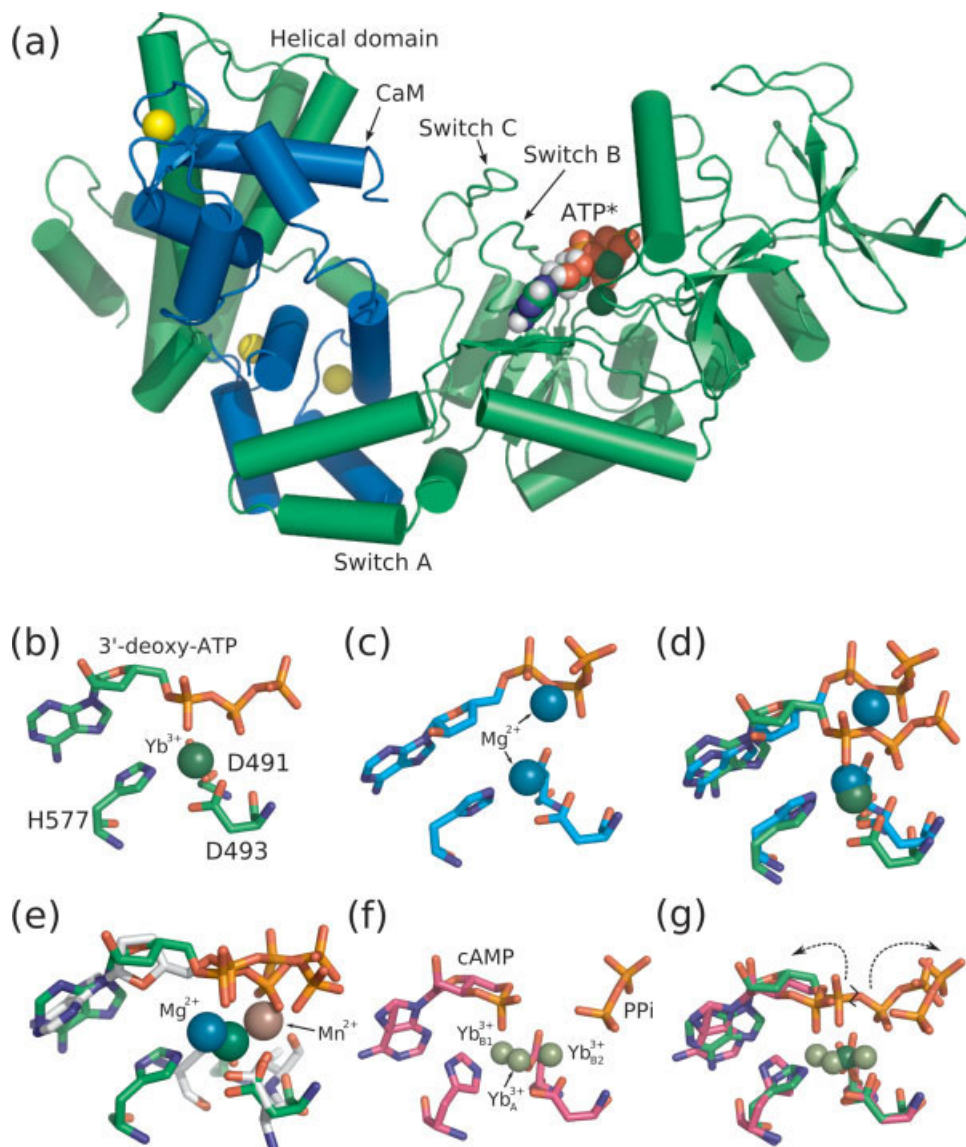
Additional Supporting Information may be found in the online version of this article.

Leandro Martínez's current address is Institute of Chemistry, State University of Campinas (UNICAMP), Sao Paulo, Brazil. Grant sponsors: The National Scientific Research Centre (CNRS), the Pasteur Institute.

\*Correspondence to: Thérèse Malliavin, Unité de Bioinformatique Structurale, URA CNRS 2185, Institut Pasteur, 28, rue du Dr. Roux, F-75015 Paris, France. E-mail: terez@pasteur.fr.

Received 26 January 2009; Revised 17 June 2009; Accepted 17 June 2009

Published online 6 July 2009 in Wiley InterScience (www.interscience.wiley.com). DOI: 10.1002/prot.22523

**Figure 1**

(a) Structure of the EF-CaM complex. (b-g) Binding modes of 3'-deoxy-ATP, PPI and cAMP observed in crystallographic structures: (b) 3'-deoxy-ATP in the presence of a single Yb<sup>3+</sup> ion (PDB entry 1K90).<sup>1</sup> (c) 3'-deoxy-ATP in the presence of two Mg<sup>2+</sup> ions (1XFV).<sup>3</sup> (d) Superposition of models *b* and *c*. (e) Superposition of *b* and the active site of the Mammalian Adenylyl Cyclase.<sup>7</sup> (f) cAMP and PPI with two different Yb<sup>3+</sup> binding modes, with one or two ions (1SK6).<sup>5</sup> (g) Superposition of *b* and *f*, suggesting that product conformations in *f* result from cyclization of ATP in *b*.

reaction, with the ATP substrate analog 3'-deoxy-ATP and for which two structures have been determined (1XFV, 1K90) and (ii) the state after the reaction, with the products cAMP and PPI (1SK6). These two states correspond to the two extremities of the enzymatic reaction path, and, consequently, are expected to have different substrate, product, and ion binding properties. Before reaction, the enzyme should bind the reactant tightly and precisely to initiate bond cleavage. After reaction it should rapidly release the products. As a consequence,

ions of the active site are expected to have different functions at each phase of the reaction.

Two substrate conformations were obtained in the structures with 3'-deoxy-ATP and were associated with different ion binding modes. Structure 1K90 was obtained with a single Yb<sup>3+</sup> ion [Fig. 1(b)]. A two-Mg<sup>2+</sup> binding mode was also observed [structure 1XFV: Fig. 1(c)], and a two-metal-ion catalytic mechanism was proposed,<sup>3</sup> similar to the one observed in Mammalian adenylyl cyclases (MACs) [Fig. 1(e)].<sup>6,7</sup> The faster cata-

**Table 1**  
Simulated Systems

Simulation group	Structural model and main system components	Production runs
1xfv-Mg1	1XFV, ATP, and the central Mg <sup>2+</sup> in the active site	10 of 1 ns
1xfv-Mg2	1XFV, ATP, and two Mg <sup>2+</sup> in the active site	10 of 1 ns
1k90-Mg1	1K90, ATP, and the central Mg <sup>2+</sup> in the active site	10 of 1 ns
1k90-Mg2	1K90, ATP, and two Mg <sup>2+</sup> in the active site	10 of 1 ns
1sk6-Mg1	1SK6, cAMP, PPI, and the central Mg <sup>2+</sup> in the active site	10 of 1 ns
1sk6-Mg2	1SK6, cAMP, PPI, and two Mg <sup>2+</sup> in the active site	10 of 1 ns

For each of these systems, 10 independent runs were performed starting with different velocity distributions. 1xfv-Mg1 and 1k90-Mg2 are auxiliary simulations that use cationic binding modes that were not directly suggested by the crystallographic models.

lytic rate of EF relative to other adenylyl cyclases support the hypothesis of a slightly different catalytic mechanism.<sup>8</sup> Indeed, EF function is to overproduce cAMP and disturb cell function, contrary to native MACs which must catalyze ATP cyclization in a cell-controlled fashion. Similarly, a mix of two Yb<sup>3+</sup> binding modes was suggested during the refinement of the structure of EF-CaM bound to the products [1SK6: Fig. 1(f)].<sup>5</sup> Therefore, EF appears to present two possible ionic binding modes, with one or two cations. The cationic binding mode has been recently shown<sup>9</sup> to be essential for the proper docking of the substrate.

The ions will be called either “central” or “non-central” according to their positions in the catalytic site. The central ion is coordinated by Asp491, Asp493, and His577. This ion is present in 1K90, 1XFV, and 1SK6 ionic binding mode of higher occupancy [Fig. 1(d,g)]. Ions in other binding positions will be referred to as non-central. These non-central ions may be the two low occupancy ions of 1SK6 or the single ion coordinated essentially by the phosphate tail of ATP in 1XFV.

In this work, molecular dynamics (MD) simulations are used to investigate the geometries and conformational variations of the active site of these structures, to obtain insights into their functional relevance. First, we present and discuss ATP binding modes. The ATP binding mode found in 1K90 appears more stable, thus suggesting that it would be closer to the reaction starting point. Then, we show that a specific combination of phosphate tail and sugar pucker conformations are required for proper orientation of the nucleophilic and electrophilic atoms involved in the cyclization reaction. Furthermore, we show that the two-metal-ion binding mode observed in 1SK6 restrains product mobility and flexibility, suggesting that the one-metal binding mode could facilitate product release.

## MATERIALS AND METHODS

### Molecular dynamics simulations

Six structural models of the EF-CaM complex were built from three crystallographic structures of PDB

entries: 1XFV, 1K90, and 1SK6, with one or two ions (Table 1). The simulations are referenced in lowercase letters (1xfv, 1k90, and 1sk6), whereas the original crystallographic structures are referenced in uppercase letters. For each simulation group, 10 runs of 1 ns were performed with different starting velocity distributions. The simulations suffixed-Mg2 were performed with two Mg<sup>2+</sup> ions in the active site, whereas those suffixed -Mg1 with one Mg<sup>2+</sup> only.

The three crystallographic structures display different active site compositions: (i) a 3'-deoxy-ATP and a Ytterbium(III) ion (1K90)<sup>1</sup>; (ii) 3'-deoxy-ATP and two Mg<sup>2+</sup> (1XFV)<sup>3</sup>; and (iii) reaction products cyclic-AMP and PPI with two alternative ion configurations containing one or two Yb<sup>3+</sup> ions (1SK6).<sup>5</sup>

Yb<sup>3+</sup> ions were replaced by Mg<sup>2+</sup> ions (the actual catalytic ion), and the missing 3'-hydroxyl of 3'-deoxy-ATP was added for the simulations. Missing residues in 1K90 (loop between K768 and F773) and in 1SK6 (loops between S674 and V694 and between Q767 and F773) were modeled based on the corresponding residues of the 1XFV structure.

The CHARMM27 force field was used for proteins, ions, and ATP.<sup>10,11</sup> Parameters for PPI and cyclic-AMP (cAMP) were derived from analogous groups in the CHARMM27 set, with Merz-Kollman charges computed using Gaussian03<sup>12</sup> from the optimized geometries at the 6-31G(d,p) level of theory. The TIP3P model was used for water.<sup>13</sup>

The structures were solvated with 25,000 water molecules yielding a water shell at least 10-Å thick (protein images being at least 20 Å apart). The water molecules were placed with Packmol,<sup>14,15</sup> as well as the sodium ions required to neutralize the system.

Energy minimizations and simulations were performed with NAMD.<sup>16</sup> The following protocols were used for equilibration. (i) The energy of the system was minimized with 2000 steps of conjugate gradients, keeping the protein, ligands and protein-bound ions fixed, except for modeled residues in 1K90 and 1SK6, which were always allowed to move. (ii) With the same atoms fixed, a 100 ps MD was performed with constant-pressure and constant-temperature conditions (NPT), with Langevin

pistons and bath to control pressure and temperature with coupling periods of 1 ps. (iii) The side-chains of the protein were allowed to move in a 500 steps conjugate gradient minimization followed by a 100 ps NPT MD. (iv) The final equilibration step was a 100 ps NPT MD without any restraint.

The equilibrated systems were about  $120 \times 80 \times 80 \text{ \AA}$  large and contains about 85,000 atoms. The production runs were performed in the NPT ensemble with periodic boundary conditions and PME electrostatics. The temperature was set to 298.15 K and the pressure to 1 Bar for all simulations. A 2 fs time-step was used and hydrogens constrained with SHAKE.<sup>17</sup>

1xfv-Mg2 was equilibrated with the two crystallographic  $\text{Mg}^{2+}$  and only the central  $\text{Mg}^{2+}$ , complexed by Asp491, Asp493, and His577, was kept for 1xfv-Mg1. 1k90-Mg2 was modeled from the equilibrated 1k90-Mg1 based on the coordination sites of the two- $\text{Yb}^{3+}$  binding mode of 1SK6. The energy of the resulting 1k90-Mg2 model was minimized with 10 conjugate gradient steps before production runs. The introduction of these ions, however, resulted in the displacement of His577 from the cation coordination site and a rotation of the adenosine group. Because of these structural distortions, the 1k90-Mg2 simulations are used only as supporting data when appropriate.

Simulations were visualized with VMD<sup>18</sup> and Figures were prepared with Pymol.<sup>19</sup> Structural alignments were performed using an orthogonal transformation.<sup>20</sup> Ribose conformations were computed according to the pseudo-rotational angle.<sup>21</sup> 3 Å distance and 20° angle were used as the cutoff to define H-bond formation, as the VMD default.<sup>18</sup> Home-made analysis programs are available at <http://lm-mdanalysis.googlecode.com>.

Water molecules with any atom within 4 Å of any solute (ATP, cAMP, and PPI) atom, were considered to form their first solvation shell. The mobility of ATP, cAMP and PPI relative to the active site was probed by monitoring the minimum distance between any of their atoms and any atom of Asp491, Asp493, and His577. These coordination residues appeared to be a good reference for this purpose because of their stable conformation and binding of the central- $\text{Mg}^{2+}$  ion.

The conformational drifts of the substrate, ATP, and of the products, cAMP and PPI, were evaluated from their RMSD from the starting coordinates in the simulation. The internal RMSDs of these molecules isolated in aqueous solution were computed from 2 ns control simulations, and oscillated around 2.0 Å for ATP, 0.6 Å for PPI, and 1.7 Å for cAMP [Supporting Information Fig. SF1].

### Estimation of the geometric fitting of $\text{Mg}^{2+}$ in the active site

The fitting of  $\text{Mg}^{2+}$  ions to the pocket geometry was qualitatively evaluated through the estimation of qualitative free energies, using the molecular mechanics Pois-

son-Boltzmann surface area (MMPBSA) method.<sup>22</sup> The MMPBSA energy is defined as:

$$\Delta G = \Delta E_{\text{MM}} + \Delta G_{\text{sol}}^{\text{polar}} + \Delta G_{\text{sol}}^{\text{nonpolar}} - T\Delta S_{\text{solute}} \quad (1)$$

where  $\Delta E_{\text{MM}}$  is the molecular mechanics contribution expressed as the sum of the electrostatics ( $\Delta E_{\text{ele}}$ ), van der Waals ( $\Delta E_{\text{vdw}}$ ) and internal ( $\Delta E_{\text{int}}$ ) energies,  $\Delta G_{\text{sol}}^{\text{polar}}$  and  $\Delta G_{\text{sol}}^{\text{nonpolar}}$  are the polar and nonpolar solvation energies, respectively.

The calculations were performed with the MMPBSA module of AMBER 9<sup>23</sup> using the ff99SB<sup>24</sup> force field. The parameters for ATP were taken from Meagher et al.<sup>25</sup> and the parameters for cAMP and PPI were computed with the ANTECHAMBER module of AMBER 9<sup>23</sup> using the AM1-BCC charge fitting.

The MMPBSA energy values were averaged along each trajectory selected for analysis. The polar contribution  $\Delta G_{\text{sol}}^{\text{polar}}$  of solvation energy was calculated by solving the Poisson-Boltzmann (PB) equation with the PBSA module of AMBER 9.<sup>23</sup> The grid spacing was set to 0.5 Å and dielectric constants of 1 and 80 were used for the interior and exterior of the solute, respectively. The dielectric boundary was defined using a 1.4 Å probe on the atomic surface. The nonpolar contribution  $\Delta G_{\text{sol}}^{\text{nonpolar}}$  was computed from the solvent accessible surface area (SASA):  $\Delta G_{\text{sol}}^{\text{nonpolar}} = 0.04356 \times \text{SASA} - 1.008$ . The solute entropy  $\Delta S_{\text{solute}}$  was not included in the total binding energy value, because of significant variances in computing this term with the MMPBSA approach.

The MMPBSA energy of magnesium binding to a receptor is defined as the energy difference between the receptor bound to  $\text{Mg}^{2+}$  and the isolated receptor and magnesium<sup>23</sup>:

$$\Delta\Delta G_{\text{bind}}(\text{Mg/receptor}) = \Delta G_{[\text{receptor-Mg}^{2+}]} - (\Delta G_{\text{receptor}} + \Delta G_{\text{Mg}^{2+}}) \quad (2)$$

Instead of calculating the  $\Delta\Delta G_{\text{bind}}(\text{Mg/receptor})$  values for magnesium binding onto different complexes and then comparing them, the differences in MMPBSA energies of magnesium between the different EF-CaM complexes were calculated directly. This way, estimation of the MMPBSA energy  $\Delta G_{\text{Mg}^{2+}}$  of a free cation in solvent was avoided.

The comparisons were made between (i) 1Mg/rec1 and 1Mg/rec2, where the MMPBSA energies were calculated on the trajectories: rec1-Mg1 and rec2-Mg1, and the same trajectories from which the magnesium ion was removed before the MMPBSA analysis, (ii) 2Mg/rec1 and 2Mg/rec2, where the MMPBSA energies were calculated on the trajectories: rec1-Mg2 and rec2-Mg2, and the same trajectories from which the two magnesium ion were removed before the MMPBSA analysis, (iii) MgC/rec1 and MgC/rec2, where the MMPBSA energies were calculated on the trajectories: rec1-Mg2 and rec2-Mg2, and the same trajectories from which the central magne-

sium ion MgC was removed before the MMPBSA analysis, (iv) MgNC/rec1 and MgNC/rec2, where the MMPBSA energies were calculated on the trajectories: rec1-Mg2 and rec2-Mg2, and the same trajectories from which the non-central magnesium ion MgNC was removed before the MMPBSA analysis. The two receptor geometries rec1 and rec2 were taken among 1xfv, 1k90, and 1sk6 for comparisons (i) and (ii), and among 1xfv and 1k90 only for comparisons (iii) and (iv).

To give an idea about the way the calculations were performed, the calculation of the energy difference  $\Delta\Delta\Delta G_{\text{bind}}(1\text{Mg}/1\text{XFV} - 1\text{Mg}/1\text{K90})$  of one  $\text{Mg}^{2+}$  between 1XFV and 1K90, is now detailed. This difference is expressed as:

$$\begin{aligned} \Delta\Delta\Delta G_{\text{bind}}(1\text{Mg}/1\text{XFV} - 1\text{Mg}/1\text{K90}) \\ = \Delta\Delta G_{\text{bind}}(1\text{Mg}/[1\text{xfv} - \text{Mg1}]) \\ - \Delta\Delta G_{\text{bind}}(1\text{Mg}/[1\text{k90} - \text{Mg1}]) \quad (3) \end{aligned}$$

was evaluated directly by reducing Eq. (3) to:

$$\begin{aligned} \Delta\Delta\Delta G_{\text{bind}}(1\text{Mg}/1\text{XFV} - 1\text{Mg}/1\text{K90}) \\ = \Delta G_{[1\text{xfv} - \text{Mg1}]} - \Delta G_{[1\text{xfv} - \text{Mg1} \setminus 1\text{Mg}]} \\ - (\Delta G_{[1\text{k90} - \text{Mg1}]} - \Delta G_{[1\text{k90} - \text{Mg1} \setminus 1\text{Mg}]}) \quad (4) \end{aligned}$$

where  $\Delta G_{[1\text{xfv} - \text{Mg1}]}$  and  $\Delta G_{[1\text{k90} - \text{Mg1}]}$  are calculated along the 1xfv-Mg1 and 1k90-Mg1 trajectories. and  $\Delta G_{[1\text{xfv} - \text{Mg1} \setminus 1\text{Mg}]}$  and  $\Delta G_{[1\text{k90} - \text{Mg1} \setminus 1\text{Mg}]}$  are calculated along the same trajectories from which one  $\text{Mg}^{2+}$  was removed.

Another kind of comparison was performed for the energy of binding between MgC and MgNC inside the same receptor geometry “rec”, chosen among 1xfv and 1k90 simulations. This comparison was performed by calculating the difference between the MMPBSA energies averaged on the trajectories rec2 - Mg2 from which the ion MgC or MgNC was alternatively removed before the MMPBSA analysis. An similar comparison between the ions  $\text{Mg}^{\text{cAMP}}$  and  $\text{Mg}^{\text{PPi}}$  bound to cAMP and to PPi was performed for 1sk6 using the simulation 1sk6-Mg2 where each ion was alternatively removed.

The comparison between MgC and MgNC is detailed in the case of the difference  $\Delta\Delta\Delta G_{\text{bind}}(\text{Mg}^{\text{C}}/1\text{XFV} - \text{Mg}^{\text{NC}}/1\text{XFV})$  for binding the central magnesium  $\text{Mg}^{\text{C}}$  and the non-central magnesium  $\text{Mg}^{\text{NC}}$  ion to 1XFV. This MMPBSA energy difference is expressed as:

$$\begin{aligned} \Delta\Delta\Delta G_{\text{bind}}(\text{Mg}^{\text{C}}/1\text{XFV} - \text{Mg}^{\text{NC}}/1\text{XFV}) \\ = \Delta\Delta G_{\text{bind}}(\text{Mg}^{\text{C}}/[1\text{xfv} - \text{Mg2}]) \\ - \Delta\Delta G_{\text{bind}}(\text{Mg}^{\text{NC}}/[1\text{xfv} - \text{Mg2}]) \quad (5) \end{aligned}$$

and can be evaluated simply by reducing Eq. (5) to:

$$\begin{aligned} \Delta\Delta\Delta G_{\text{bind}}(\text{Mg}^{\text{C}}/1\text{XFV} - \text{Mg}^{\text{NC}}/1\text{XFV}) \\ = \Delta G_{[1\text{xfv} - \text{Mg2} \setminus \text{Mg}^{\text{NC}}]} - \Delta G_{[1\text{xfv} - \text{Mg2} \setminus \text{Mg}^{\text{C}}]} \quad (6) \end{aligned}$$

where  $\Delta G_{[1\text{xfv} - \text{Mg2} \setminus \text{Mg}^{\text{C}}]}$  and  $\Delta G_{[1\text{xfv} - \text{Mg2} \setminus \text{Mg}^{\text{NC}}]}$  are the MMPBSA energies calculated on the 1xfv trajectories from which either the central magnesium  $\text{Mg}^{\text{C}}$  or the non-central magnesium  $\text{Mg}^{\text{NC}}$  was removed.

## RESULTS

### ATP binding modes

As described in the introduction, a two-metal ion bound EF structure (1XFV) has been obtained,<sup>3</sup> apparently unifying the description of the binding pockets of EF and other Adenylyl Cyclases. Nevertheless, some features of 1XFV do not fully support this common mechanism. First, the 3'-deoxy-ATP conformation and  $\text{Mg}^{2+}$  positions in the 1XFV structure [Fig. 1(c)] are different from those observed in MACs. In particular, two Aspartates coordinate both cations in MACs<sup>7</sup> while, in 1XFV, these conserved Aspartates only bind the central- $\text{Mg}^{2+}$ . The second ion interacts with the phosphate tail of 3'-deoxy-ATP and is more than 3.5 Å away from any atom of the protein<sup>3</sup> [Fig. 1(c)]. Second, an inspection of the electronic density of this  $\text{Mg}^{2+}$  in 1XFV revealed that it can be confused with that of the 3'-deoxy-ATP phosphate tail [Supporting Information Fig. SF2b], or with a water molecule, which bears the same number of electrons. Third, the distance of the phosphate oxygens to the central- $\text{Mg}^{2+}$  is about 5 Å, and the latter can only weakly stabilize the phosphate charges in this configuration.

In fact, the unfavorable incorporation of the second  $\text{Mg}^{2+}$  ion in 1XFV and the nonstandard docking of 3'-deoxy-ATP could be due to the large concentration of  $\text{Mg}^{2+}$ , 200 mM, used to grow crystals. This concentration is largely above that required to fully inhibit the catalytic activity of EF.<sup>2</sup> Therefore, the conformation found in 1XFV would be inactive and probably distorted.

MD simulations 1xfv-Mg2, 1xfv-Mg1, and 1k90-Mg1 were used to analyze the active site configurations with one or two  $\text{Mg}^{2+}$  ions, and with different observed ATP conformations. Because of steric clashes (described in Materials and Methods), the simulation 1k90-Mg2 will be used for comparison purposes only.

The interaction energies between the molecules were used to monitor the proximities between the partners and thus the geometry of the active site. In 1xfv-Mg2, ATP interacts with the non-central  $\text{Mg}^{2+}$  with a calculated interaction energy of about  $-936 \text{ kcal mol}^{-1}$ , whereas the calculated interaction energy with the central- $\text{Mg}^{2+}$  is about  $-360 \text{ kcal mol}^{-1}$  [Fig. 2(a)]. Removing the non-central ion does not change significantly the interaction of ATP to the central- $\text{Mg}^{2+}$  [Fig. 2(a), 1xfv-Mg1], and no transition promoting a stronger interaction was observed in 1xfv-Mg1 runs.

In 1k90-Mg1, the interaction energy between ATP and the central- $\text{Mg}^{2+}$  was about  $-736 \text{ kcal mol}^{-1}$ , almost two times stronger than in 1xfv simulations [Fig. 2(b,c)].

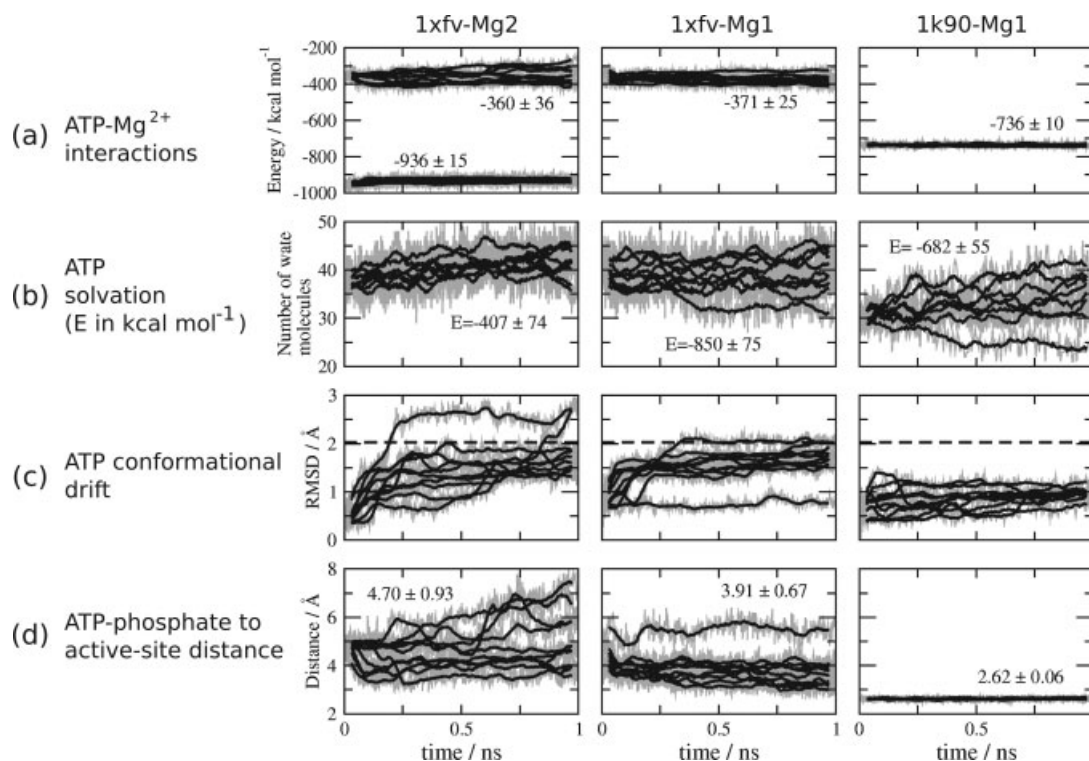


**Figure 2**

Energetics and dynamics of ATP binding. (a) Interactions of ATP with  $\text{Mg}^{2+}$  ions (average interaction energies are given in  $\text{kcal mol}^{-1}$ ). (b) Solvation of ATP as given by the number of water molecules in the first solvation shell and average interaction energies. (c) Conformational drift of ATP in the active site. The dashed lines indicate the RMSD of ATP isolated in water. (d) Distance between the phosphate group of ATP and the coordination site of the central- $\text{Mg}^{2+}$ , distance values are given in Å.

This stronger ATP interaction is due to the conformation of the phosphate tail of ATP, the other components of the active site having similar contributions in 1k90 and 1xfv [Fig. 1(d)].

Interaction of ATP with water varied among 1xfv-Mg2, 1xfv-Mg1, and 1k90-Mg1 simulations [Fig. 2(b)]. On the one hand, the number of water molecules in the first solvation shell of ATP in 1xfv-Mg2 and in 1xfv-Mg1 was around 40, and was only slightly smaller in 1k90-Mg1. On the other hand, the interaction energies were stronger with a single  $\text{Mg}^{2+}$  (1xfv-Mg1:  $-850 \text{ kcal mol}^{-1}$  and 1k90-Mg1:  $-682 \text{ kcal mol}^{-1}$ ) than with two  $\text{Mg}^{2+}$  (1xfv-Mg2:  $-407 \text{ kcal mol}^{-1}$ ). Therefore, the single- $\text{Mg}^{2+}$  binding mode favored the direct interaction of water molecules with ATP.

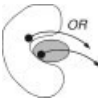
In a way similar to the approach described earlier for the calculated interaction energies, MMPBSA interaction energies of ions  $\text{Mg}^{2+}$  with the system were calculated. The range of obtained values, as well as the fluctuations, are far from expected free energy values (Table II), but they can be used to analyze in a qualitative way the direct interactions and the fitting of the ions to the pocket geometry. The advantage of using the MMPBSA approach with respect to a simple calculation of the mo-

lecular mechanics interaction energy is that the inclusion of the Poisson-Boltzmann solvation energy takes into account the relaxation of water molecules when an ion is removed.

The MMPBSA energies of interaction of the  $\text{Mg}^{2+}$  ions computed during the simulations 1k90 and 1xfv were compared (Table II) using the MMPBSA methodology, as described in Materials and Methods. The following perturbations were studied: (i) the removal of the central ions in the one ion-binding mode, (ii) the simultaneous removal of two ions, (iii) the removal of one ion in the two ion-binding mode, (iv) the binding of the central ion MgC closest to the enzyme, and (v) the binding of the non-central ion MgNC closest to ATP. The 1K90 geometry display the most favorable MMPBSA energy values for all considered comparisons. This suggests that the cavity geometry in 1K90 is the most favorable to the binding of  $\text{Mg}^{2+}$ , and is in agreement with the stronger interaction energies observed between partners in that case. Then the binding of the central ion and the non-central ions was compared and, in both 1K90 and 1XFV cavities, the MMPBSA energy is more favorable for the central ion. This observations suggests that the central ion is firmly bound and that the non-central

**Table II**

MMPBSA Energies Used to Evaluate Fitting of Magnesium Ions to the Different Structures of the EF-CaM Complex, or to the Different Sites of the Same Structure

Compared systems	$\Delta\Delta\Delta G$ (kcal/mol)	Perturbation
1Mg/1XFV – 1Mg/1K90	195 ± 33	
1Mg/1XFV – 1Mg/1SK6	-37 ± 32	
1Mg/1K90 – 1Mg/1SK6	-232 ± 37	
2Mg/1XFV – 2Mg/1K90	293 ± 88	
2Mg/1XFV – 2Mg/1SK6	70 ± 26	
2Mg/1K90 – 2Mg/1SK6	-223 ± 94	
Mg <sup>C</sup> /1XFV – Mg <sup>NC</sup> /1XFV	-49 ± 16	
Mg <sup>C</sup> /1K90 – Mg <sup>NC</sup> /1K90	-78 ± 68	
Mg <sup>cAMP</sup> /1SK6 – Mg <sup>PPi</sup> /1SK6	-29 ± 13	
Mg <sup>C</sup> /1XFV – Mg <sup>C</sup> /1K90	121 ± 44	
Mg <sup>NC</sup> /1XFV – Mg <sup>NC</sup> /1K90	92 ± 56	

The standard deviations provided represent the technical fluctuations in the calculations. “1Mg” denotes the simulations performed with one ion, “2Mg” with two ions. Mg<sup>C</sup> and Mg<sup>NC</sup> denote the central and non-central ions present in the 1K90 and 1XFV geometry. Mg<sup>cAMP</sup> and Mg<sup>PPi</sup> are the ions bound to cAMP and PPi, respectively.

Mg<sup>2+</sup> is probably less tightly bound, depending on the current state of the enzyme complex and also on ion concentration. The more favorable Mg<sup>2+</sup> ion binding in 1K90 suggests a single cation mechanism.

Similarly, the analysis of the dynamics of ATP in the binding site suggests a tighter docking of the substrate in 1K90 relative to 1XFV. The conformational drift of ATP was analyzed by calculation of the RMSD from its initial conformation. This quantity is about 2 Å for ATP isolated in solution (Supporting Information Fig. SF1). In all EF-CaM complexes, the conformational drift was reduced [Fig. 2(c)]. Furthermore, in 1k90-Mg1, the drift of ATP was systematically smaller than in the 1xfv simulations, indicating a tighter docking of ATP.

This tighter docking can be explained by the stronger binding of the phosphate tail of ATP to the central-Mg<sup>2+</sup> ion, observed above in 1k90-Mg1 [Fig. 2(a)]. Furthermore, the distances of the phosphate tail of ATP to the Mg<sup>2+</sup>-coordination site were not only smaller but also displayed much smaller oscillations in 1k90-Mg1 than in 1xfv simulations [Fig. 2(d)]. Therefore, the interaction of the ATP tri-phosphate group to the central-Mg<sup>2+</sup> ion was structurally more stable in 1k90-Mg1, which can be

correlated with the more favorable MMPBSA energy of this ion in 1K90 relative to other binding site geometries.

The average mobility of the adenosine atoms of ATP relative to the active site residues was similar in all simulations as indicated by the average distances of about 3.0 Å, but displayed slightly more fluctuations in 1k90-Mg1 (Supporting Information Fig. SF3). By contrast, the distance of the ribose group of ATP to the coordination site, was slightly larger, and fluctuated more in 1k90-Mg1 (4.3 ± 0.9 Å) than in 1xfv simulations (1xfv-Mg2: 3.8 ± 0.7 Å, 1xfv-Mg1: 3.7 ± 0.6 Å) (Supporting Information Figure SF3). This larger mobility of ribose and adenosine groups observed in 1k90-Mg1, indicates that the restrained mobility of ATP in the 1k90-Mg1 simulations comes from the tighter binding of the phosphate tail of ATP only.

To summarize, the interactions of ATP with the central-Mg<sup>2+</sup> are more effective in 1K90 than in 1XFV. This provides an argument in favor of single-Mg<sup>2+</sup> binding modes, but we will see below that a two-cation binding might favor the nucleophilic attack. Nevertheless, we suggest that the ATP conformation observed in the 1K90 model is closer to the reaction starting point. The similarities of this conformation with the substrate conformation in MACs [Fig. 1(e)] and with the conformation of reaction products [1SK6: Fig. (g)] support this interpretation.

### Nucleophilic attack, sugar pucker and phosphate conformations

The essential step in the cyclization catalyzed by MACs, also proposed for EF, is the nucleophilic attack of the P $\alpha$  phosphorous by the ribose O3' oxygen, which leads to the cycle formation and PPi release. But, to prevent cyclization and trap the reactant, the crystal structures have been obtained with an analog lacking the O3' oxygen, which makes difficult to connect the analysis of the active site to a mechanistic analysis of the reaction. Consequently, we tried here not to evaluate the effective free energy barriers of reaction, but to sort the initial cavity geometry in terms of their propensity to favor the O3' to P $\alpha$  approach.

Therefore, we will use the O3'-P $\alpha$  distance as an indication of the similarity of the ATP docking conformation to the one required for the initiation of the reaction. Fig. 3(a) represents the conformations of ATP observed in crystallographic structures, with modeled O3' atoms. The distance between the O3' and P $\alpha$  atoms in 1K90 is 3.6 Å, more favorable for nucleophilic attack than it is in 1XFV (4.2 Å). The analysis of the simulations showed that this interpretation was too simplistic and also provided a richer view of the conformational conditions that could initiate nucleophilic attack, as we shall see below.

Fig. 3(b) shows the probability of finding the O3' and P $\alpha$  atoms within a given distance. The probability of finding the atoms within 4 Å is significant in 1xfv-Mg2

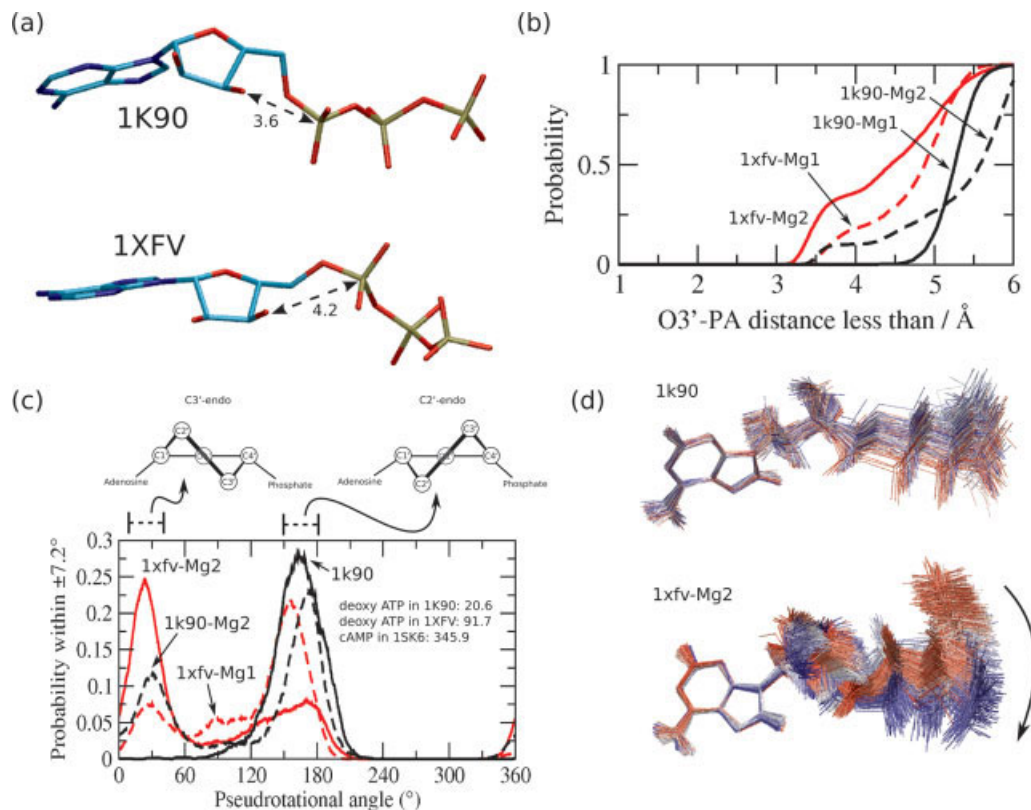


**Figure 3**

(a) Modeling of the O3' oxygen on the ATP conformations observed in crystallographic models and their distances (Å) to P $\alpha$ . (b) Probability of finding the P $\alpha$  atom within a given distance of the O3' in each set of simulations. (c) Ribose conformations in each system, as indicated by the pseudo-rotational angle parameter ( $p$ ).<sup>21</sup> The  $p$  values observed in the crystallographic structures are indicated. (d) Phosphate tail conformations observed in the superposition of simulation snapshots from 1k90 and 1xfv-Mg2. The structures are colored from red to blue from the start to the end of the run.

and quite lower for 1k90-Mg1. Therefore, these simulations suggested an opposite trend to that of the crystallographic structures. This trend was inverted in 1xfv-Mg1 when a Mg<sup>2+</sup> was removed, or in 1k90-Mg2 with an additional Mg<sup>2+</sup>. The removal of an ion in 1xfv increased the distance between O3' and P $\alpha$ , whereas the addition of the second Mg<sup>2+</sup> to 1k90 broadened the distance distribution. Therefore, the presence of two ions appeared to shift the distribution to smaller distances, where the nucleophilic attack should be facilitated.

The analysis of the ribose and phosphate conformations in these simulations provided a refined picture of the structural requirements allowing an effective reaction. Fig. 3(c) shows the conformational regions sampled by the ribose group in each set of simulations. The two most common sugar conformations<sup>21</sup> were populated: the C3'-endo region, corresponding to a pseudo-rotational angle,  $p$ , between 0 and 36°, and the C2'-endo region, with  $p$  between 144 and 180°.

In 1xfv-Mg2 the ribose was essentially found in the C3'-endo conformation, which brought O3' close to P $\alpha$ .

Upon non-central-Mg<sup>2+</sup> removal, in 1xfv-Mg1, the population was significantly shifted towards the C2'-endo conformation. A parallel effect was observed for 1k90 simulations: in 1k90-Mg1 the conformation was C2'-endo exclusively, but the addition of a second ion allowed the apparition of some C3'-endo conformers.

Therefore, the simulations indicated that the ribose conformation depends on the Mg<sup>2+</sup> population in the binding site and has a strong impact on the O3'-P $\alpha$  distance. The presence of a second ion in the active site, either in 1xfv-Mg2 or in 1k90-Mg2, also tends to favor the C3'-endo conformation because of the attractive interactions between ATP O3' and the second cation. One should notice that the shift toward the C3'-endo conformation occurs for a second ion being added both to 1xfv-Mg2 or 1k90-Mg2 non-central ion positions, which differ from each other [Fig. 1(c,f)].

Simulations 1k90-Mg1 and 1xfv-Mg2 yielded different ribose conformations than those observed in corresponding crystallographic structures: C3'-endo in 1K90 and O1'-endo ( $p \sim 90^\circ$ ) in 1XFV. As the change in ribose

conformation from O1'-endo in 1XFV to C3'-endo only affected the O3'-P $\alpha$  distance by about 0.02 Å, it could not account for the O3'-P $\alpha$  distance reduction in 1xfv-Mg2. Other relative motions of the sugar and the phosphate tail must have occurred. This hypothesis is supported by the observations made on the electronic density of 1XFV [Supporting Information Fig. SF2b]: while the electronic density does not provide a clear determination of the sugar pucker, the phosphate tail is clearly positioned. In the simulations, the conformational drifts of the phosphate tail from the crystallographic structure revealed a greater flexibility in 1xfv than in 1k90-Mg1 and 1k90-Mg2 [Fig. 2(c)]. Drifts were also smaller in 1k90-Mg2 than in 1xfv-Mg2 but larger than in 1k90-Mg1 (data not shown). To decipher which crystallographic structure would display an initial geometry more favorable for an O3'-P $\alpha$  approach, it was controlled whether conformations with small O3'-P $\alpha$  distance in 1xfv-Mg2 had a phosphate tail conformation similar to that of 1XFV.

The analysis of ATP binding modes [Fig. 2(c,d)] showed that ATP was highly mobile in 1xfv-Mg2 simulations, and that the phosphate tail drifted away from the active site. Fig. 3(d) illustrates the phosphate tail motions by the superposition of the snapshots of respectively a typical 1k90-Mg1 run and a typical 1xfv-Mg2 run, colored along time from red (start) to blue (end). In 1k90-Mg1, the phosphate tail essentially oscillates around an average conformation, whereas, in 1xfv-Mg2, it drifts systematically away from the crystallographic position. The greater O3'-P $\alpha$  proximity in 1xfv-Mg2 is produced by a drift from the 1XFV crystallographic conformation.

The presence of two-Mg<sup>2+</sup> favored the C3'-endo ribose pucker by attraction of the O3' oxygen towards the phosphate group. Two auxiliary simulations were performed, each one containing five runs, one in which the ribose conformation was restrained to C3'-endo with a force constant of 500 kcal mol<sup>-1</sup> rad<sup>-2</sup>, the other in which the O3'-P $\alpha$  distance was restrained to 3.0 Å with a force constant of 50 kcal mol<sup>-1</sup> Å<sup>-2</sup>. Restraining the ribose conformation to C3'-endo reduced the O3'-P $\alpha$  distance, whereas restraining the O3'-P $\alpha$  distance induces the C3'-endo pucker. This clearly showed the link between the ribose pucker and the O3'-P $\alpha$  distance.

The comparison of 1XFV and 1K90, and of the corresponding simulations in presence of one or two Mg<sup>2+</sup> ions, allowed to draw the following conclusions. First, the conformation C3'-endo decreases the distance between O3' and P $\alpha$ , which should favor a geometry more prone to efficient nucleophilic attack. Second, the presence of two ions in the simulations induces a shift in the sugar pucker toward C3'-endo and, consequently, the nucleophilic attack would be easier. Nevertheless, the large drift of the phosphate tail observed in 1xfv simulations suggests that the two-ion binding mode would only

favor the nucleophilic attack in a conformation that has drifted away from that of 1XFV.

### A two-Mg<sup>2+</sup> binding mode significantly restrained product mobility

The crystal structures of the 3'-deoxy-ATP-EF-CaM complex (1XFV, 1K90) all display a clearly observable central ion, coordinated by Asp491, Asp493, and His577 (Fig. 1 and Supporting Information Fig. SF2a,b). By contrast, the structure 1SK6, containing the reaction products, displays two Yb<sup>3+</sup> binding modes [Fig. 1(f)]. In one binding mode (80% occupancy), a single Yb<sup>3+</sup> ion occupies a central position, in coordination with Asp491, Asp493, and His577, with a similar geometry to that observed for the central-Mg<sup>2+</sup> of 1XFV and 1K90. A better fitting of the electronic density (Supporting Information Fig. SF2c) is obtained if a two-Yb<sup>3+</sup> binding mode is also considered at lower occupancy (20%).<sup>5</sup> This configuration resembles that observed in the two-metal-ion catalytic domain of Mammalian adenylyl cyclases,<sup>5,7</sup> where Aspartates coordinate both cations. However, several features of the structure 1SK6, as the low resolution (3.2 Å), and the large differences between R and R<sub>free</sub> (Supporting Information Table ST), introduce uncertainties on the relevance of the two-Yb<sup>3+</sup> binding mode. Additionally, the small distance between the two Yb<sup>3+</sup> ions, less than 4 Å, implies a large electrostatic repulsion (~750 kcal mol<sup>-1</sup>), although it can be alleviated by the proximity of the phosphate groups of cAMP and PPi.

To evaluate the relevance of the two binding modes, molecular dynamics simulations were performed starting from 1SK6, and replacing the Yb<sup>3+</sup> ions by Mg<sup>2+</sup> ions. The simulations containing the two-ion and the one-ion binding modes were named 1sk6-Mg2 and 1sk6-Mg1, respectively.

The interaction energies of the products with the Mg<sup>2+</sup> ions were in direct relation with the distances between them [Fig 4(a)]. In 1sk6-Mg2, PPi interacted with the Mg<sup>2+</sup> ions with averages energies of  $-426 \pm 13$  and  $-741 \pm 21$  kcal mol<sup>-1</sup> for the ions farther and closer to PPi, respectively. The interaction of PPi with the central-Mg<sup>2+</sup> in 1sk6-Mg1 was  $-467 \pm 25$  kcal mol<sup>-1</sup>. Similarly, cAMP interaction energies in 1sk6-Mg2 were  $-270 \pm 5$  and  $-112 \pm 6$  kcal mol<sup>-1</sup> for the Mg<sup>2+</sup> closer and farther from cAMP, respectively. Surprisingly, the cAMP-Mg<sup>2+</sup> interactions in 1sk6-Mg1 was less favorable than for either ion in 1sk6-Mg2 and displayed large fluctuations ( $-100 \pm 31$  kcal mol<sup>-1</sup>). Furthermore, along the runs, a systematic weakening of the interaction was observed [Fig. 4(a), cAMP in 1sk6-Mg1].

Stronger product-protein and product-water interactions were observed in the one-ion binding mode (1sk6-Mg1) than in the two-ion binding mode (1sk6-Mg2), similarly to what was observed for ATP simulations. The interactions with the protein strengthened from  $-104$  to

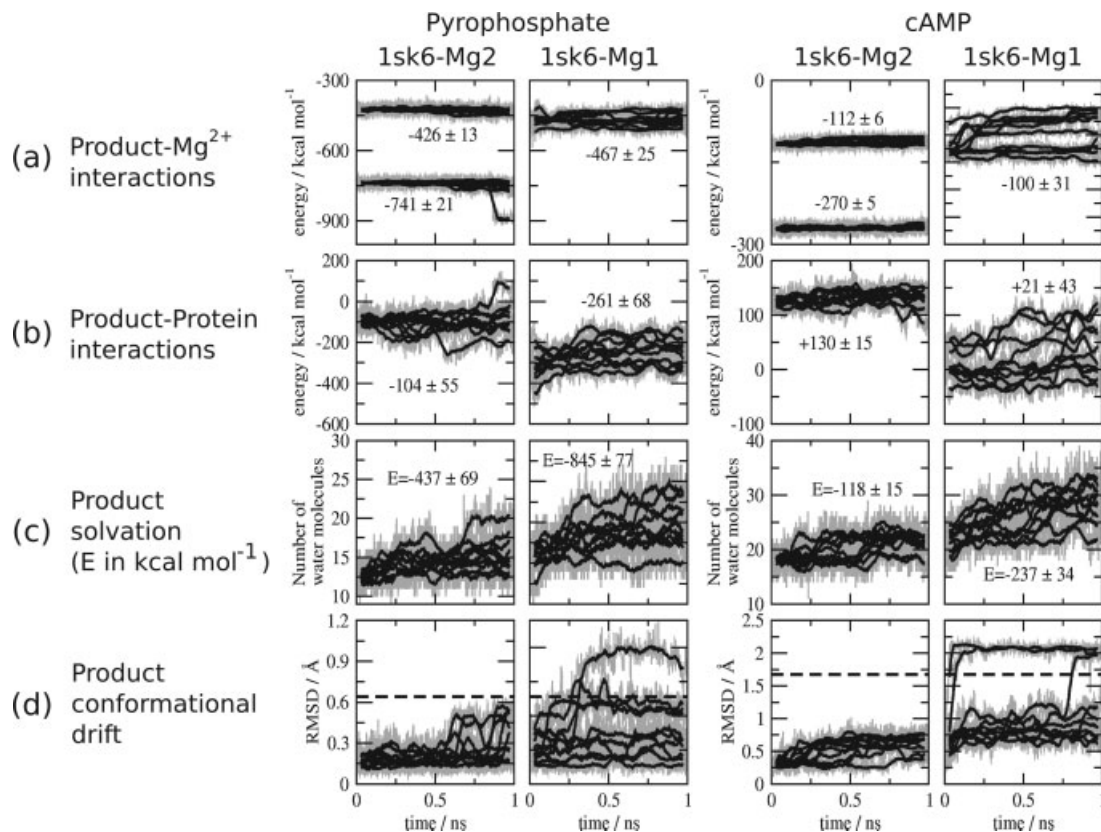


**Figure 4**

Energetics and conformational drift of product binding. (energies are given in  $\text{kcal mol}^{-1}$ ). (a) Interaction of PPI and cAMP with the active site  $\text{Mg}^{2+}$  ions. (b) Product-protein interactions. (c) Product solvation defined as the number of water molecules in their first solvation shell (associated average interaction energies with water are indicated). (d) Conformational drifts ( $\text{\AA}$ ). Dashed lines indicate average RMSD in solution.

$-261 \text{ kcal mol}^{-1}$  for PPI and from  $+130$  to  $+21 \text{ kcal mol}^{-1}$  for cAMP upon  $\text{Mg}^{2+}$  removal. Similarly, the PPI-water interactions improved from  $-437$  to  $-485 \text{ kcal mol}^{-1}$  and the cAMP-water interactions from  $-118$  to  $-237 \text{ kcal mol}^{-1}$ . These energetic effects were accompanied by larger energy fluctuations and a larger number of first shell water molecules. Therefore, the removal of one  $\text{Mg}^{2+}$  promoted enhanced interactions with water and with the protein, but an overall more flexible binding.

The MMPBSA energies of interaction of the  $\text{Mg}^{2+}$  ions in the 1SK6 cavity geometry were compared (Table II) with the ones obtained for the cavities from 1K90 and 1XFV. A larger binding instability was observed in 1SK6 with one ion, which indicates a weakening of the interactions at the end of the reaction, when their catalytic role is accomplished. Nevertheless, in the case where the simultaneous binding of two ions is considered, a better energy of interaction is observed for 1SK6 than for 1XFV. This is in agreement with the quite unfavorable geometry observed in 1XFV and the very high  $\text{Mg}^{2+}$  concentration necessary to crystallize this structure. The comparison of the MMPBSA difference energy between  $\text{Mg}^{\text{cAMP}}$  and  $\text{Mg}^{\text{PPI}}$

in the 1SK6 cavity indicates that the fitting of the ion is slightly more favorable when it is bound to cAMP.

The mobilities of cAMP and PPI were reduced in the active site as compared with that in bulk water [Fig. 4(d)]. The conformational drifts were lower in 1sk6-Mg2 than in 1sk6-Mg1. Additionally, in three 1sk6-Mg1 runs, the bending of the base relative to the ribose group of cAMP resulted in larger conformational deviations relative to the initial cAMP conformation.

The mobilities of the products with respect to the  $\text{Mg}^{2+}$ -coordination site residues were affected when the ion binding mode was changed (Fig. 5). The distance of PPI from the coordination site displayed larger averages and standard deviations in 1sk6-Mg1, revealing weaker ion-PPI interactions than in 1sk6-Mg2 [Fig. 5(a,b)]. In 1sk6-Mg1, the bound conformation of PPI was stabilized by hydrogen bonds with the side-chains of three Lysine residues: K346 (75% of the time), K353 (72%), and K372 (51%), and with the amide nitrogen of Ser354 (59%). Thus, the Lysines played an important role in stabilizing the PPI group, but they also impaired its dissociation in the time-scale of these simulations. However, proton

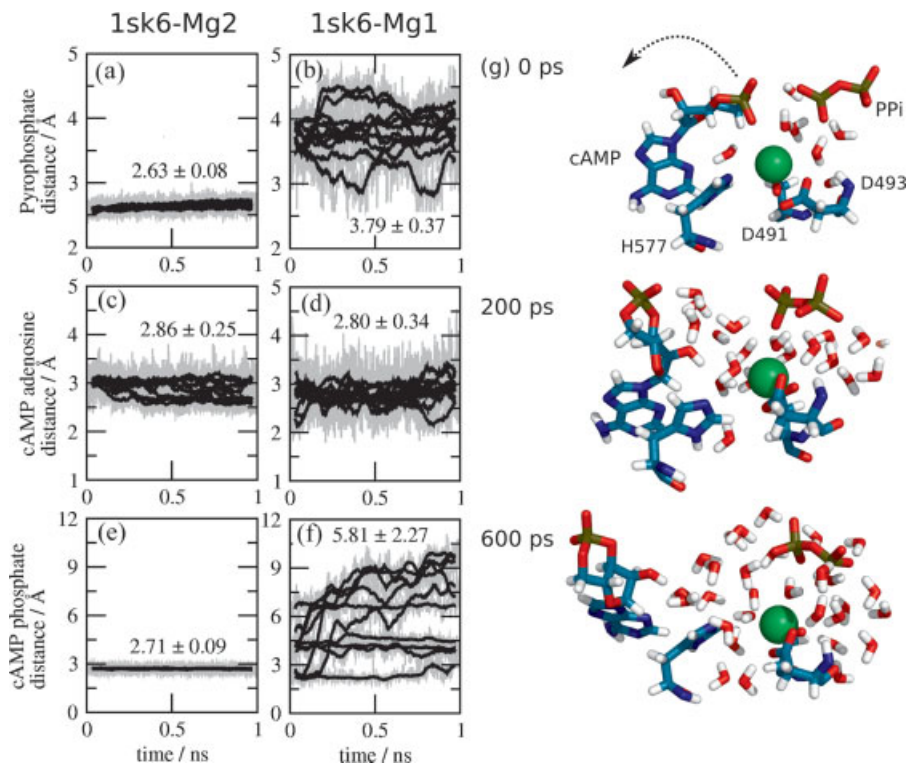


**Figure 5**

(a-f) Distances of the reaction products from the  $Mg^{2+}$  coordination site residues. The mean value and standard deviation are written on each panel. (g) Snapshots of one of the 1sk6-Mg1 runs in which a partial dissociation of cAMP was observed. The dissociation and entrance of water molecules in the active site occurred simultaneously (not all water molecules are shown).

transfer from these Lysine side-chains to PPI could occur, first helping electron transfer in the catalytic reaction, then reducing PPI charge and thus its interactions with the  $Mg^{2+}$  ion. The reduction of PPI charge can facilitate its dissociation.

The distance of the cAMP phosphate group to the coordination site remained essentially constant in 1sk6-Mg2 [Fig. 5(e)], but varied significantly in 1sk6-Mg1, yielding different profiles for each run and increasing up to 9 Å [Fig. 5(f)]. These variations reflected initial stages of dissociation of cAMP from the active site in 1sk6-Mg1 [Fig. 5(g)], and are correlated most of the time with a weakening in cAMP- $Mg^{2+}$  interaction energies [Fig. 4(a)]. The dissociation of cAMP did not proceed further as the adenosine group of cAMP maintained its interactions with the binding site (mixed hydrophilic and hydrophobic interactions with L348, G547, T548, G578, T579, D582, N583). Consequently, the distance of the cAMP adenosine relative to the active site was not significantly perturbed.

To summarize, the two- $Mg^{2+}$  binding mode restrained product flexibility and mobility relative to the central- $Mg^{2+}$  binding site, and prevented the dissociation trend observed for cAMP in 1sk6-Mg1.

## DISCUSSION

The MD simulations presented above permitted to draw a picture of the relevance of the number of ions and of the substrate conformations observed in ground state before and after the cyclization reaction. As the structures displaying one or two  $Mg^{2+}$  ions were obtained with different substrate conformations, it is difficult to dissociate the effects of the ion-binding and of the substrate-binding mode.

Therefore, we cannot from the present study give definitive arguments to decide whether the enzyme could work with either one or two bound metals. The adenylyl cyclase EF display a turnover<sup>3</sup> of  $1000 \text{ sec}^{-1}$ , which is several millions times slower than the turnover of a diffusion-controlled reaction (Superoxide dismutase:  $7 \times 10^9 \text{ sec}^{-1}$ ). This suggests that the conformation of the reactants are not tightly constrained in the protein active site and that the analysis of the relevance of the different reaction players, performed here, is a mandatory preliminary step to sort out the different possibilities.

The single-ion binding mode in 1k90-Mg1 allowed a tight binding of the substrate. On the other hand, less stable ATP conformations were observed for 1k90 with

two ions as well as in the 1XFV geometry. The destabilization of ATP binding by an improper incorporation of a second ion could explain the total inhibition of the enzyme at high  $Mg^{2+}$  concentrations.<sup>2</sup> The inhibition of product dissociation in the presence of two  $Mg^{2+}$  could also contribute to this inhibitory effect, as suggested by the results of 1sk6-Mg2 compared with those of 1sk6-Mg1.

We interpret these results as an indication that the ATP conformation observed in the 1K90 structure would be the most probable starting point for the reaction. Indeed, the extended phosphate-tail conformation, observed in 1K90, would allow a better docking of ATP than the bent conformation of 1XFV. An argument in favor of the extended tail conformation as the pre-reaction form is that the structure 1SK6 of EF bound to reaction products seems to result from a reaction starting from the 1K90 structure [Fig. 1(g)]. A second argument is that the 1K90 binding mode resembles that of Mammalian Adenylyl Cyclases (MACs). The choice of the ATP conformation observed in 1K90, as a starting point of the reaction, would reconcile the conformations of the substrate observed in EF with those of the substrates in MACs.

An additional argument in favor of the geometry of the active site in 1K90 arises from the amino-acid composition of EF and MACs. Indeed, the phosphate group of the substrates is stabilized in MACs by three basic residues (two Arginines and one Lysine), whereas an additional Lysine is present in EF (three Lysines and one Arginine, Supporting Information Fig. SF4). The presence of this additional basic residue could allow the enzyme to work with a single catalytic ion, and is then an argument in favor of the conformations observed in 1K90.

On the other side, the presence of two  $Mg^{2+}$  in the binding site allowed a sugar pucker and phosphate tail conformations better suited for O3'-P $\alpha$  approach. From this point of view, the single-ion binding mode observed in 1K90 seems less favorable. The absence to date of a 1K90-like structure with two  $Mg^{2+}$  could be due to the missing O3' oxygen in 3'-deoxy-ATP. Indeed, O3' should make an important interaction with the additional  $Mg^{2+}$  ion, which in turn would have induced additional relaxation of the active site. Such interaction was formed in 1k90-Mg2 simulations, where a second  $Mg^{2+}$  ion was placed in a geometry similar to those of the product-bound structure 1SK6.

In presence of two  $Mg^{2+}$  ions, conformational drifts, mobilities and dissociation events of the products were reduced compared with the system with one  $Mg^{2+}$ , because both PPI and cAMP are tightly bound to one of the ions. As the two-ion binding mode significantly stabilizes the binding of reaction products and, thus, reduces the efficiency of the enzyme, the presence of two highly charged  $Yb^{3+}$  in the crystal of 1SK6 might have trapped the products in the active site. Finally, the dynamics of the products suggested a mechanistic interpre-

tation that may help to understand EF function. Indeed, if two ions could actually be transiently necessary for the enzymatic reaction, the breaking of product-ion bonds would be a limiting step for product release.

Although only indicative, the MMPBSA energies of  $Mg^{2+}$  binding are in agreement with a relaxed shape of the cavity in 1K90, for which the best binding energies are observed in all considered binding cases. This is also in agreement with the better conformation observed for ATP in the cavity 1K90. The binding of the central ion is always more favorable than the binding of the ion closer to the substrate. This could support a view of the catalytic mechanism where one ion is present in the enzyme cavity before the substrate loading, and plays a major role in the reaction mechanism.

## CONCLUSION

The main conclusion of the manuscript is that among the conformation of ATP, the most efficient potential starting point for the reaction appears that observed in 1K90. The structure 1K90 was obtained in the presence of one ion only. This suggests that the presence of two ions would not be mandatory for EF function, although this could be due to the use of a modified ATP molecules for crystallization purposes. A transient two-ion binding mode cannot be ruled out because the proper sugar pucker appears to be induced by the presence of a second ion in the binding site. However, the evidences supporting a one-ion mechanism are more convincing: (i) The amino-acid composition of EF's active site support the possibility of a one-ion binding site relative to MACs. (ii) The 1K90-like extended phosphate tail conformation facilitates O3' to P $\alpha$  approach, and reduces the ATP's conformational flexibility. (iii) The central-ion is tightly bound to the catalytic site, and interacts strongly with the substrate. (iv) 1XFV, which contains two ions, was obtained with a  $Mg^{2+}$  concentration which fully inhibits the enzyme. (v) Finally, our simulations also suggest that the presence of two ions impairs the dissociation of the reaction products from 1SK6. The single-ion mechanism could be behind the high turnover rate and unregulated ATP cyclization in EF relative to MACs.<sup>2</sup>

## ACKNOWLEDGMENTS

LM thanks the Coordenação de Aperfeiçoamento de Pessoal de Nível Superior (CAPES) of Brazil for a post-doctoral fellowship. EL thanks the French Ministry of Defence (DGA/MRIS) (DGA/CNRS PhD support).

## REFERENCES

1. Drum CL, Yan SZ, Bard J, Shen Y, Lu D, Soelaiman S, Grabarek Z, Bohm A, Tang WJ. Structural basis for the activation of anthrax adenyl cyclase exotoxin by calmodulin. *Nature* 2002;415:396–402.

- Shen Y, Lee YS, Soelaiman S, Bergson P, Lu D, Chen A, Beckingham K, Grabarek Z, Mrksich M, Tang WJ. Physiological calcium concentrations regulate calmodulin binding and catalysis of adenylyl cyclase exotoxins. *EMBO J* 2002;21:6721–6732.
- Shen Y, Zhukovskaya NL, Guo Q, Florian J, Tang WJ. Calcium-independent calmodulin binding and two-metal-ion catalytic mechanism of anthrax edema factor. *EMBO J* 2005;24:929–941.
- Laine E, Yoneda JD, Blondel A, Malliavin TE. The conformational plasticity of calmodulin upon calcium complexation gives a model of its interaction with the oedema factor of *Bacillus anthracis*. *Proteins* 2008;71:1813–1829.
- Guo Q, Shen Y, Zhukovskaya NL, Florian J, Tang WJ. Structural and kinetic analyses of the interaction of anthrax adenylyl cyclase toxin with reaction products cAMP and pyrophosphate. *J Biol Chem* 2004;279:29427–29435.
- Kamenetsky M, Middelhaufe S, Bank EM, Levin LR, Buck J, Steegborn C. Molecular Details of cAMP generation in mammalian cells: a tale of two systems. *J Mol Biol* 2006;362:623–639.
- Tesmer JJ, Sunahara RK, Johnson RA, Gosselin G, Gilman AG, Sprang SR. Two-metal ion catalysis in adenylyl cyclase. *Science* 1999;285:756–760.
- Tang WJ, Krupinski J, Gilman AG. Expression and characterization of calmodulin-activated (type i) adenylyl cyclase. *J Biol Chem* 1991;266:8595–8693.
- Chen D, Menche G, Power TD, Sower L, Peterson JW, Schein CH. Accounting for ligand-bound metal ions in docking small molecules on adenylyl cyclase toxins. *Proteins* 2007;67:593–605.
- MacKerell AD, Bashford D, Bellott M, Dunbrack RL, Evanseck JD, Field MJ, Fischer S, Gao J, Guo H, Ha S, Joseph-McCarthy D, Kuchnir L, Kuczera K, Lau FTK, Mattos C, Michnick S, Ngo T, Nguyen DT, Prodhom B, Reiher WE, Roux B, Schlenkrich M, Smith JC, Stote R, Straub J, Watanabe M, Wiorkiewicz-Kuczera J, Yin D, Karplus M. All-atom empirical potential for molecular modeling and dynamics studies of proteins. *J Phys Chem B* 1998;102:3586–3616.
- Pavelites JJ, Bash PA, Gao J, MacKerell AD. A molecular mechanics force field for NAD<sup>+</sup>, NADH and the pyrophosphate groups of nucleotides. *J Comput Chem* 1997;18:221–239.
- Frisch MJ, Trucks GW, Schlegel HB, Scuseria GE, Robb MA, Cheeseman JR, Montgomery, Jr JA, Vreven T, Kudin KN, Burant JC, Millam JM, Iyengar SS, Tomasi J, Barone V, Mennucci B, Cossi M, Scalmani G, Rega N, Petersson GA, Nakatsuji H, Hada M, Ehara M, Toyota K, Fukuda R, Hasegawa J, Ishida M, Nakajima T, Honda Y, Kitao O, Nakai H, Klene M, Li X, Knox JE, Hratchian HP, Cross JB, Bakken V, Adamo C, Jaramillo J, Gomperts R, Stratmann RE, Yazev O, Austin AJ, Cammi R, Pomelli C, Ochterski JW, Ayala PY, Morokuma K, Voth GA, Salvador P, Dannenberg JJ, Zakrzewski VG, Dapprich S, Daniels AD, Strain MC, Farkas O, Malick DK, Rabuck AD, Raghavachari K, Foresman JB, Ortiz JV, Cui Q, Baboul AG, Clifford S, Cioslowski J, Stefanov BB, Liu G, Liashenko A, Piskorz P, Komaromi I, Martin RL, Fox DJ, Keith T, Al-Laham MA, Peng CY, Nanayakkara A, Challacombe M, Gill PMW, Johnson B, Chen W, Wong MW, Gonzalez C, Pople JA. Gaussian 03, Revision C02. Gaussian: Wallingford, CT: 2004.
- Jorgensen WL, Chandrasekhar J, Madura JD, Impey RW, Klein ML. Comparison of simple potential functions for simulating liquid water. *J Chem Phys* 1983;79:926–935.
- Martínez JM, Martínez L. Packing optimization for automated generation of complex system's initial configurations for molecular dynamics and docking. *J Comput Chem* 2003;24:819–825.
- Martínez L, Andrade R, Birgin EG, Martínez JM. PACKMOL: A package for building initial configurations for molecular dynamics simulations. *J Comput Chem* 2009;30:2157–2164.
- Phillips JC, Braun R, Wang W, Gumbart J, Tajkhorshid E, Villa E, Chipot C, Skeel RD, Kale L, Schulten K. Scalable molecular dynamics with NAMD. *J Comput Chem* 2005;26:1781–1802.
- Ryckaert JP, Ciccotti G, Berendsen HJC. Numerical integration of the cartesian equations of motion of a system with constraints: molecular dynamics of *n*-alkanes. *J Comp Phys* 1977;23:327–341.
- Humphrey W, Dalke A, Schulten K. VMD—visual molecular dynamics. *J Molec Graphics* 1996;14:33–38.
- DeLano WL. The pymol molecular graphics system. DeLano Scientific, Palo Alto, CA, 2002. Available at: <http://www.pymol.org>.
- Kearsley SK. On the orthogonal transformation used for structural comparisons. *Acta Cryst A* 1989;45:208–210.
- Altona C, Sundaralingam M. Conformational analysis of the sugar ring in nucleosides and nucleotides a new description using the concept of pseudotation. *J Am Chem Soc* 1972;94:8205–8212.
- Srinivasan J, Cheatham TE, Cieplak JP, Kollman PA, Case DA. Continuum solvent studies of the stability of DNA, RNA, and phosphoramidate—DNA helices. *J Am Chem Soc* 1998;120:9401–9409.
- Case DA, Darden TA, Cheatham TE, Simmerling CL III, Wang J, Duke RE, Luo R, Merz KM, Pearlman DA, Crowley M, Walker RC, Zhang W, Wang B, Hayik S, Roitberg A, Seabra G, Wong KF, Paesani F, Wu X, Brozell S, Tsui V, Gohlke H, Yang L, Mongan J, Hornak V, Cui G, Beroza P, Mathews DH, Schafmeister C, Ross WS, Kollman PA. AMBER 9. San Francisco: University of California; 2006.
- Hornak V, Abel R, Okur A, Strockbine B, Roitberg A, Simmerling C. Comparison of multiple Amber force fields and development of improved protein backbone parameters. *Proteins* 2006;65:712–725.
- Meagher KL, Redman LT, Carlson HA. Development of polyphosphate parameters for use with the AMBER force field. *J Comput Chem* 2003;24:1016–1025.